FULL PAPER

From Black Phosphorus to Phosphorene: Basic Solvent Exfoliation, Evolution of Raman Scattering, and Applications to Ultrafast Photonics

Zhinan Guo, Han Zhang, Shunbin Lu, Zhiteng Wang, Siying Tang, Jundong Shao, Zhengbo Sun, Hanhan Xie, Huaiyu Wang, Xue-Feng Yu,* and Paul K. Chu*

Although phosphorene has attracted much attention in electronics and optoelectronics as a new type of two-dimensional material, in-depth investigations and applications have been limited by the current synthesis techniques. Herein, a basic *N*-methyl-2-pyrrolidone (NMP) liquid exfoliation method is described to produce phosphorene with excellent water stability, controllable size and layer number, as well as in high yield. Phosphorene samples composed of one to four layers exhibit layer-dependent Raman scattering characteristics thus providing a fast and efficient means for the in situ determination of the thickness (layer number) of phosphorene. The linear and nonlinear ultrafast absorption behavior of the as-exfoliated phosphorene is investigated systematically by UV–vis–NIR absorption and Z-scan measurements. By taking advantage of their unique nonlinear absorption, ultrashort pulse generation applicable to optical saturable absorbers is demonstrated. In addition to a unique fabrication technique, our work also reveals the large potential of phosphorene in ultrafast photonics.

1. Introduction

In the wake of the discovery of graphene, a two-dimensional (2D) material with outstanding mechanical,[1] electrical,[2–4] carrier transport,[5] and thermal properties,[6] many other types of 2D materials, such as transition metal dichalcogenides (TMDs), transition metal oxides (TMOs), and black phosphorus (BP) have aroused great interest.[7–10] These 2D materials are composed of individual layers held together by van der Waals forces in lieu of covalent or ionic bonds that are found in most materials. Using a physical or chemical method, the bulk materials can be exfoliated down to a few layers or even a monolayer and the optical, phonon, and electronic properties of the materials change dramatically as a result. As a common technique to impart molecular vibrational information, Raman scattering has been used to characterize the layer number,[11] edges,[12] and strain[13,14] of graphene and other 2D materials.

Black phosphorus has great potential in electronics and optoelectronics due to its bandgap structure, which is tunable by varying the thickness, its high carrier mobility, and its anisotropic photoelectronic properties.[15–23] The bandgap of bulk BP is 0.3 eV but can be extended to 1.5 eV in monolayered phosphorene commonly referred to as BP atomic layers. The wide-range adjustability and direct bandgap of BP are expected to emulate graphene in optoelectronics.[24] The thickness (layer number) of BP is an important parameter and it has been reported that both the field-effect mobility and current on/off ratio depends on it.[17] Raman scattering conveys valuable information about BP as a result of the three distinct peaks corresponding to the A_g^1, B_{2g}, and A_g^2 vibrational modes of the phosphorus atoms in BP and the crystal orientation,[25] strain,[26] thickness,[27] temperature,[28] and angular[28,29] dependent Raman characteristics have been widely studied. Typically, R. Martel et al. have reported the Raman properties of mono-, bi-, and multilayer phosphorene and its thickness-related effects. They have found that the Raman peak position and width-at-half-maximum of the A_g^2 mode are sensitive to the layer number of phosphorene.[27] Y. Lu et al. have studied the temperature-dependent Raman properties of phosphorene, and have demonstrated that few-layer phosphorene is more sensitive to temperature modulation than graphene and MoS_2. Also, they have reported the anisotropic Raman response

Dr. Z. Guo, Prof. H. Zhang, Dr. S. Lu, Dr. Z. Wang, Dr. J. Shao, Dr. Z. Sun
SZU-NUS Collaborative Innovation Center for
Optoelectronic Science and Technology
Key Laboratory of Optoelectronic Devices and Systems of Ministry
of Education and Guangdong Province
College of Optoelectronic Engineering
Shenzhen University
Shenzhen 518060, P. R. China
E-mail: hzhang@szu.edu.cn

DOI: 10.1002/adfm.201502902

S. Tang, H. Xie, Prof. H. Wang, Prof. X.-F. Yu
Institute of Biomedicine and Biotechnology
Shenzhen Institutes of Advanced Technology
Chinese Academy of Sciences
Shenzhen 518055, P. R. China
E-mail: xf.yu@siat.ac.cn
Prof. P. K. Chu
Department of Physics and Materials Science
City University of Hong Kong
Tat Chee Avenue
Kowloon, Hong Kong, P. R. China

© 2015 WILEY-VCH Verlag GmbH & Co. KGaA, Weinheim

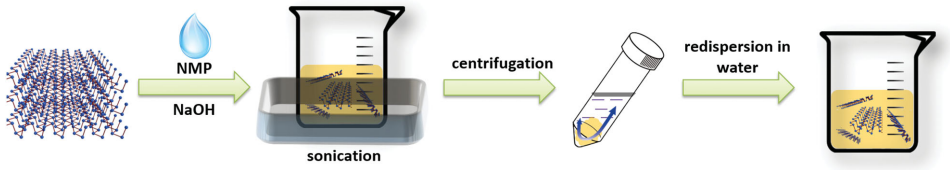

Figure 1. Schematic illustration of the fabrication process of basic-NMP-exfoliated phosphorene.

in few-layer phosphorene, which enables us to use such optical method to quickly determine the crystalline orientation.[28] In this paper, the layer-dependent Raman shifts and intensities of three typical vibrational modes A_g^1, B_{2g}, and A_g^2 of phosphorene are investigated.

Phosphorene with only a few layers is generally prepared by mechanical cleavage, which is also a common technique for producing graphene from graphite. Although physical exfoliation is useful for fundamental research, the large-scale production of 2D materials with a few layers is difficult. Another way to prepare phosphorene is liquid phase exfoliation in a solvent such as *N*-methyl-2-pyrrolidone (NMP).[30] This method enables the large-scale exfoliation of BPs and a uniform dispersion in the exfoliation medium, such as NMP. However, the production yield by this method is generally low and the obtained phosphorene is not stable in other conventional solvents, such as water, thereby hampering the applications of phosphorene. In this paper, we describe a basic-NMP solvent exfoliation technique for the high-yield production of phosphorene with a high stability in water. The ability of synthesizing these materials in large quantities in a controllable manner enables the in-depth investigation of their Raman properties, as well as their linear and nonlinear optical properties.

2. Results and Discussions

2.1. Basic Solvent Exfoliation in NMP

A basic-NMP solvent exfoliation method was designed to prepare phosphorene as shown in **Figure 1**. In brief, bulk BP was added to a saturated NaOH NMP solution, which was put in a sonicator for 4 h to conduct liquid exfoliation. After sonication, the phosphorene in NMP was separated and transferred to water by centrifugation.

Figure 2 depicts photographs of the NMP and water solutions containing the phosphorene that was exfoliated in NMP (without NaOH) and basic-NMP solvent (with NaOH). All the solutions were obtained from the exfoliation of bulk BP with the same weight. Comparing the color of the solutions between bottles (b) and (d), a more efficient BP exfoliation can be observed from the basic-NMP than with the pure NMP. The

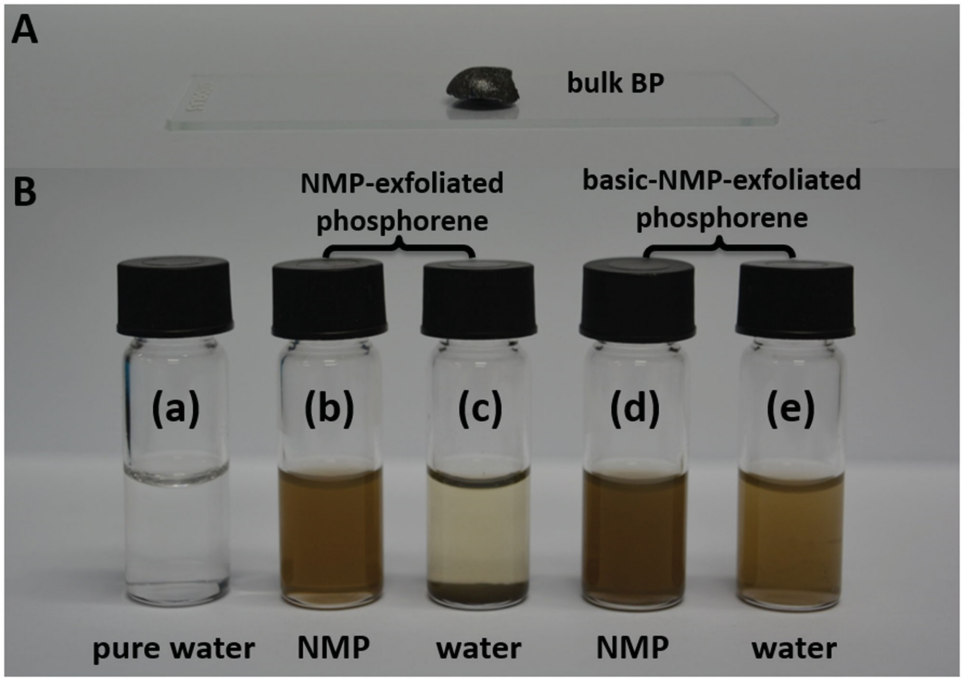

Figure 2. Photographs of A) bulk BP and B) phosphorene dispersed in NMP and water. The five bottles shown in (B) contain: a) pure water, b) NMP-exfoliated phosphorene in NMP, c) NMP-exfoliated phosphorene in water, d) basic-NMP-exfoliated phosphorene in NMP, and e) basic-NMP-exfoliated phosphorene in water.

© 2015 WILEY-VCH Verlag GmbH & Co. KGaA, Weinheim

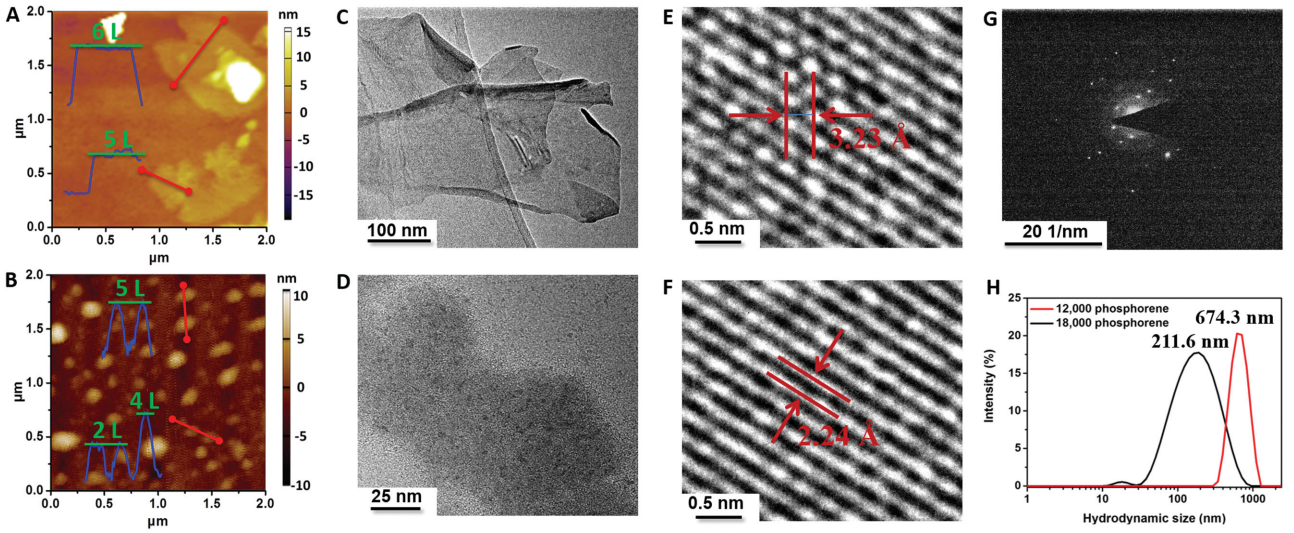

Figure 3. Height-mode AFM images of A) 12 000 and B) 18 000 phosphorene; TEM images of C) 12 000 and D) 18 000 phosphorene; E,F) HR-TEM images of phosphorene with different crystal lattices; G) SAED pattern of phosphorene. H) Size distributions of 12 000 and 18 000 phosphorene determined by dynamic light scattering.

basic-NMP-exfoliated phosphorene exhibits an excellent stability in both NMP and water. The zeta potential of the basic-NMP-exfoliated phosphorene was −30.9 mV and that of the NMP-exfoliated one was only −19.7 mV (Figure S1, Supporting Information). Generally, a suspension with a zeta potential of over 30 mV (absolute value) is physically stable and it can thus be inferred that the basic-NMP-exfoliated phosphorene with a favorable negative charge is stable in water. Here, the negative charge of the phosphorene comes from the OH^- ions in the liquid exfoliation system by adding NaOH. These OH^- ions are absorbed on the surface of phosphorene, which results in a negative charge, and thus causes the excellent stability in water. NMP is a good solvent to carry out the exfoliation of 2D materials[30,31] but as it is an organic solvent with poor volatility, phosphorene extracted by an NMP solution cannot be used directly in the fabrication of electronic devices or for optical investigations. The improved basic-NMP-exfoliation method described here overcomes these hurdles enabling subsequent systematic investigations.

Similar to mechanical exfoliation, liquid exfoliation cannot produce 2D materials with an exact size and thickness. In order to produce phosphorene with a relatively uniform size and thickness, the phosphorene dispersion was centrifuged at different speeds. As shown in **Figure 3**, the statistical AFM and dynamic light scattering show that the phosphorene obtained by centrifugation at 12 000 rpm (designated 12 000 phosphorene) had an average diameter of about 670 nm and a thickness of 5.3 ± 2.0 nm (5–12 layers). The supernatant was then further centrifuged at 18 000 rpm to obtain phosphorene with an average diameter of around 210 nm and a thickness of 2.8 ±1.5 nm (2–7 layers, designated 18 000 phosphorene). 68% of the 18 000 phosphorene had a thickness of around 1.5–2.5 nm corresponding to 2–4 layers (Figure S2, Supporting Information). There are some small flakes in the 18 000 phosphorene that could not be observed in the height-mode AFM images but that are visible in phase-mode AFM images (Figure S3, Supporting Information), suggesting that these flakes are monolayered phosphorene, which are too thin for the AFM instrument to capture. The results suggest that the thickness of phosphorene can be controlled by regulating the centrifugal speed. Here, the obtained 18 000 phosphorene and 12 000 phosphorene represent two kinds of products with a significant difference in thickness. Figure S4 in the Supporting Information displays the height-mode AFM image of NMP-exfoliated phosphorene without adding NaOH. Only 6–10 nm (10–16 layers) thick flakes were found, no few-layered flakes were obtained without NaOH. These results disclose that a more thorough exfoliation of BP is achieved by the basic-NMP process rather than by NMP-only exfoliation. The 18 000 phosphorene, which is thinner than the 12 000 phosphorene, was chosen for subsequent optical evaluation.

Transmission electron microscopy (TEM) was performed to examine the morphology and crystallinity of the phosphorene. An ultrathin nanosheet of phosphorene with stacked folds is revealed in Figure 3C. The crystallinity of the phosphorene was studied by high-resolution TEM (HR-TEM) (Figure 3E and 3F) and selected-area electron diffraction (SAED) (Figure 3G). Clear lattice fringes were observed from the BP atomic layer and those of 3.23 Å (Figure 3E) and 2.24 Å (Figure 3F) correspond to the (012) and (014) planes of the BP crystal, respectively, which is consistent with well-known BP lattice parameters.[32] The uniform lattices shown in Figure 3E and 3F suggest that the phosphorene produced by basic-NMP-exfoliation retains the original crystalline state. It should be noted that it is difficult to obtain high-quality SAED patterns because the electron beam destroys the crystalline BP changing it to the amorphous form during data acquisition.

2.2. Layer-dependent Raman Scattering

Figure 4 shows the Raman characteristics of phosphorene samples with different amounts of layers. In order to acquire Raman scattering from phosphorene with an exact layer number,

© 2015 WILEY-VCH Verlag GmbH & Co. KGaA, Weinheim

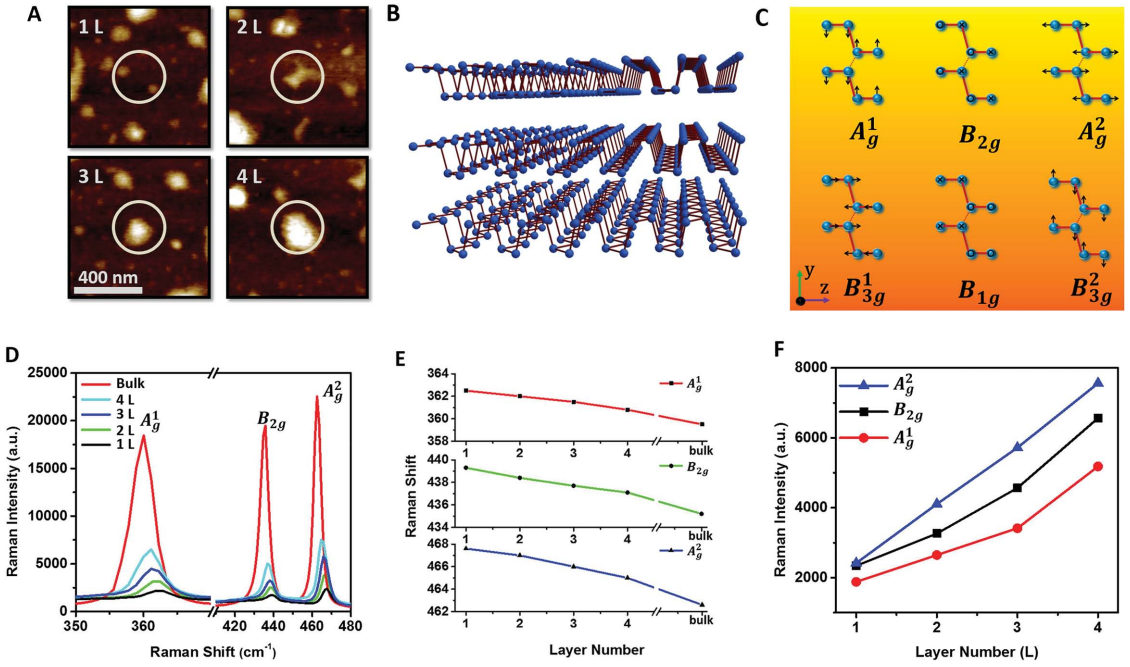

Figure 4. A) Height-mode AFM images of 1–4 L phosphorene; B) 2D view of the layered BP structure; C) Atomic displacement of the Raman active modes in BP; D) Raman spectra of bulk BP and phosphorene with different numbers of layers; E) Layer-dependent Raman peak shift in phosphorene; F) Layer-dependent Raman peak enhancement.

silicon wafers with markers were used. After obtaining the height-mode AFM images, the sample was transferred directly to the *XY* motorized sample stage of the Raman spectrometer so that Raman spectra could be acquired from an area with the same layer number. A 100× objective lens with NA = 0.90 was used and the size of the 633-nm laser was about 300 nm. Figure 4A depicts the AFM images of 1–4 L phosphorene for Raman characterization.

It is known that the phosphorus atoms within a layer of phosphorene are covalently bonded by sp^3 hybridization. The three electrons on one P atom bond with three other P atoms covalently and one lone pair is left. Hence, monolayered phosphorene has the structure of a quadrangular pyramid as illustrated in Figure 4B. According to the conservation of momentum and the group theory, there are six Raman active modes of the 12 lattice vibrational modes as shown in Figure 4C, but only three vibrational modes A_g^1, B_{2g}, and A_g^2 can be detected when the incident laser is perpendicular to the layered phosphorene plane. As shown in Figure 4D, there are three Raman peaks at 362.5 cm^{-1}, 439.3 cm^{-1}, and 467.6 cm^{-1} from the monolayered phosphorene corresponding to the A_g^1, B_{2g}, and A_g^2 modes, respectively. As the layer number of phosphorene increases, the three Raman peaks red-shift and the layer-dependent Raman shifts are summarized in Figure 4E. Among the three vibrational modes, the A_g^2 mode is the most sensitive to the number of layers and when the layer number increases from 1 L to 4 L, the A_g^2 mode red-shifts from 467.6 cm^{-1} to 465.0 cm^{-1}.

The layer-dependent Raman shifts are consistent with density functional theory calculations obtained by Wan et al.[33] The mechanism is described as follows. Under the influence of covalent bonding, the P atoms collectively oscillate within the monolayer. When another layer of phosphorene is added and bonded by van der Waals forces, the oscillation of the P atoms is hindered. Hence, the corresponding Raman energy becomes smaller resulting in a red-shift. Here, the interlayer van der Waals force, which is dominant along the stacking direction in BP, plays an important role in the layer-dependent Raman characteristics. When the layer number increases, both the low-frequency rigid phosphorene layer breathing mode and shear mode red-shift and the correction on the interlayer van der Waals forces becomes weak. Therefore, the shift from the monolayered phosphorene to the bilayered phosphorene is the largest. A further increase in the layer number produces relatively lower shifts as exemplified by the B_{2g} shear mode. The B_{2g} mode deviation between 1 L and 2 L phosphorene is 1.0 cm^{-1}, but that between 3 L and 4 L is only 0.6 cm^{-1}. The layer-dependent Raman shifts can be effectively utilized to determine the thickness of phosphorene in situ similar to graphene.

Layer-dependent Raman intensities can also be observed from phosphorene (see Figure 4F). The intensities of the A_g^1, B_{2g}, and A_g^2 modes increase with the number of layers from 1 L to 4 L and the results are consistent with those in the literature.[10] It is known that the absolute Raman intensity varies with the instrument used and even the same Raman instrument may produce different Raman intensities under different instrumental conditions. Hence, it is suggested that layer-dependent Raman intensities should only be used as a secondary tool to determine the phosphorene thickness. In our study, the three Raman peaks of phosphorene are normalized with respect to the standard silicon Raman peak (520.7 cm^{-1}) (see Figure S5, Supporting Information) and should not change from instrument to instrument. So the accuracy of the Raman peak location can be guaranteed. Consequently, any Raman

© 2015 WILEY-VCH Verlag GmbH & Co. KGaA, Weinheim

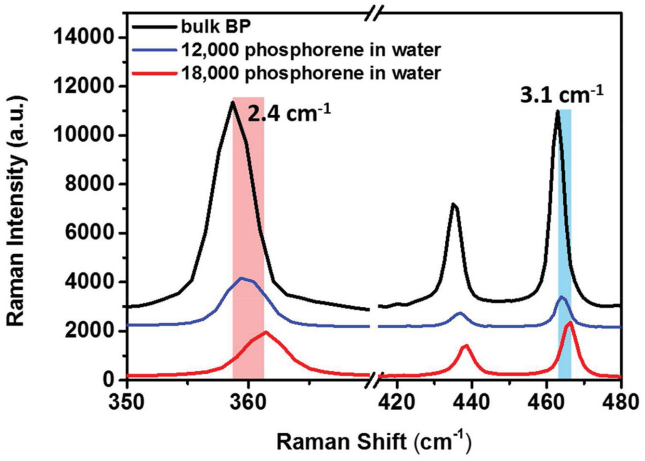

Figure 5. Raman spectra acquired from the 12 000 and 18 000 phosphorene in water.

instrument with an accuracy of around 0.5 cm^{-1} can be used to identify the thickness of phosphorenes.

The Raman spectra of phosphorene in water are shown in **Figure 5**. The Raman peaks from 12 000 and 18 000 phosphorene exhibit a certain degree of blue shift compared to bulk BP and that of the 18 000 phosphorene solution is larger because the average thickness is smaller. The results demonstrate that the Raman peak location does not only provide accurate information about the layer number of phosphorene on the silicon wafer, but can also be used to determine the average thickness of phosphorene in the solution.

2.3. Application to Ultrafast Photonics

As predicted theoretically, phosphorene has a thickness-dependent direct bandgap which changes from 0.3 eV in the bulk to 1.5 eV in a monolayer. UV–vis–NIR spectrophotometry was employed to determine the absorption properties of phosphorene (**Figure 6**). Three absorption peaks at 310, 380, and 470 nm were observed. The 310 nm peak is consistent with

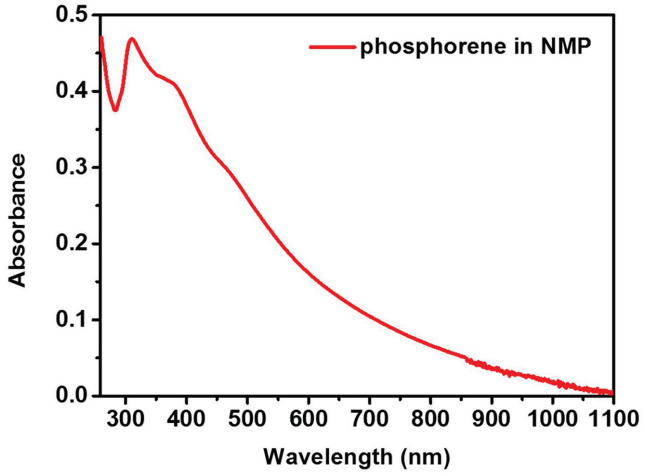

Figure 6. Absorption spectra of phosphorene in NMP.

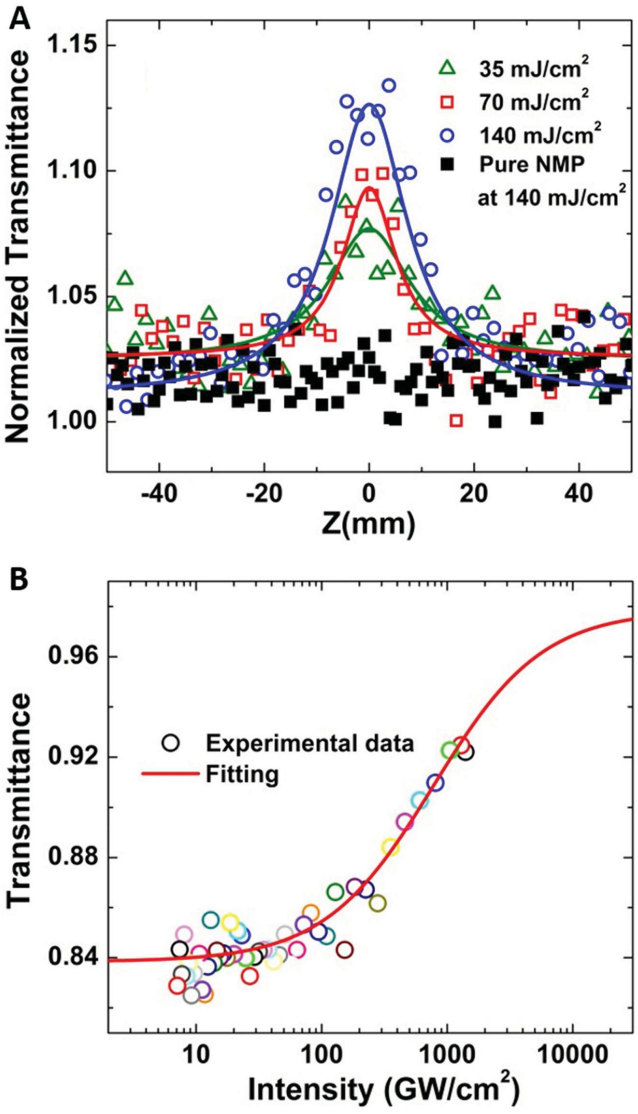

Figure 7. A) Open-aperture Z-scan measurements of phosphorene dispersions at 800 nm. B) Relationship between transmittance of the phosphorene dispersions and intensity of the femtosecond laser.

previous results obtained from black phosphorus quantum dots by Zhang et al.[34]

Ultrafast nonlinear absorption by the phosphorene dispersions was investigated by the Z-scan technique.[35,36] A mode-locked Ti:sapphire oscillator-seeded regenerative amplifier was used to generate femtosecond pulses with a peak wavelength of 800 nm, pulse width of 100 fs, and repetition rate of 1 kHz. The open-aperture Z-scan measurements are shown in **Figure 7**A. Typical saturable absorption curves were observed under excitation by an 800-nm laser. In order to exclude the effects of the NMP dispersion and the 1-mm cuvette, pure NMP was also measured but no nonlinear absorption was found providing evidence that phosphorene itself does have saturable absorption at 800 nm. The relationship between the transmittance and the incident intensity is shown in Figure 7B based on fitting the data using the following formula:[37]

© 2015 WILEY-VCH Verlag GmbH & Co. KGaA, Weinheim

$$T = 1 - \frac{\alpha_s}{1 + \frac{I}{I_s}} - \alpha_{ns}, \quad (1)$$

where α_s and α_{ns} are the saturable and nonsaturable absorption, respectively, I is the incident intensity, and I_s the saturable intensity defined as the intensity required in a steady state to reduce the absorption to half of its value. The saturable intensity and modulation depth were fitted to 774.4 GW cm^{-2} and 14.2%, respectively. The nonlinear optical absorption by phosphorene could be exploited in a saturable absorber and Q-switcher in ultrafast photonics.

The optical saturable absorption could be exploited in ultrafast photonics applications. By integrating phosphorene onto the end-facet of an optical fiber pigtail, a new optical saturable absorber could be fabricated. By adopting the same thought behind a graphene saturable absorber, previously reported by ourselves,[38] a prototype was produced by placing the optical device inside a fiber laser cavity. For more details about the performance of the phosphorene-based optical saturable absorber, please refer to the Supporting Information.

3. Conclusion

A basic-NMP liquid exfoliation method was designed to produce phosphorene with an excellent water stability and controllable size and layer number in large quantities. As the layer number increased, the A_g^1, B_{2g}, and A_g^2 Raman peaks redshifted, thereby providing a fast and effective in situ technique to determine the thickness (layer number) of phosphorene. The linear and ultrafast nonlinear optical properties determined by UV–vis–NIR absorption spectrophotometry and Z-scan technique revealed that the chemically exfoliated phosphorene has great potential in optoelectronics. By taking advantage of the unique nonlinear absorption, ultrashort pulse generation applicable to optical saturable absorbers was demonstrated.

4. Experimental Section

Chemicals and Reagents: High-purity black phosphorus crystals were purchased from Smart Elements and NMP (99.5%) and sodium hydroxide (NaOH) were obtained from Aladdin Reagents. All the chemicals were used as received without further purification. Ultrapure deionized water (18 MΩ) was produced by a Milli-Q water purification system (Millipore Corporation, Billerica, MA, USA).

Sample Preparation: Bulk black phosphorus (15 mg) was added to the saturated NaOH/NMP solution (30 mL). The mixture was put in a sonicator operated at 40 kHz frequency and 80% power for 4 hours to conduct the liquid exfoliation of the bulk BP. After exfoliation, the solution was centrifuged at 3000 rpm for 10 min to remove any non-exfoliated bulk BP. The supernatant was then centrifuged at 12 000 rpm for another 20 min to separate the relatively thick phosphorene (5–12 layers, called 12 000 phosphorene) from the NMP. The supernatant was further centrifuged at 18 000 rpm for 20 min to separate the thinner phosphorene (1–7 layers, called 18 000 phosphorene) from the supernatant. The precipitations obtained by the two separation processes were redispersed in water and the solutions were washed by deionized water. Finally, 0.05 mL of the thick and thin phosphorene water solutions were dropped onto silicon with a 280-nm SiO_2 surface layer (1 cm × 1 cm). Subsequent characterization was carried out on silicon after drying in a vacuum dryer.

Characterization: The topography and thickness of the phosphorene were determined using a MFP-3D-S atomic force microscope (Asylum Research, USA) in the AC mode (tapping mode) in air using a PPP-NCHR probe (Nanosensors) with a nominal tip radius of less than 7 nm. Transmission electron microscopy (TEM), high-resolution bright-field TEM, and selected-area electron diffraction (SAED) were carried out using a field-emission FEI-F20 at 200 kV. The absorption spectra were acquired on a TU-1810 UV–vis–NIR spectrophotometer (Purkinje General Instrument Co. Ltd. Beijing, China). The size distribution and zeta potentials were determined on a Zetasizer Nano ZS (Malvern Instruments Ltd., UK) at 25 °C. Raman scattering was performed on a Horiba Jobin-Yvon LabRam HR-VIS high-resolution confocal Raman microscope equipped with a 633-nm laser as the excitation source at room temperature and a *XYZ* motorized sample stage controlled by LabSpec software. A 100× objective lens with a NA of 0. 90 was used thereby making the spot size of the 633-nm laser to be about 300 nm.

Supporting Information

Supporting Information is available from the Wiley Online Library or from the author.

Acknowledgements

Z.N.G. and H.Z. contributed equally to this work, which was jointly supported by the National Natural Science Foundation of China ((Grant No. 61222505, 61435010 and 51372175), Science and Technology Key Project of Shenzhen (JCYJ20140417113430608), and City University of Hong Kong Applied Research Grant (ARG) No. 9667104.

Received: July 14, 2015
Revised: September 9, 2015
Published online: October 21, 2015

[1] C. Lee, X. Wei, J. W. Kysar, J. Hone, *Science* **2008**, *321*, 385.
[2] A. H. Castro Neto, F. Guinea, N. M. R. Peres, K. S. Novoselov, A. K. Geim, *Rev. Mod. Phys.* **2009**, *81*, 109.
[3] K. S. Novoselov, A. K. Geim, S. V. Morozov, D. Jiang, Y. Zhang, S. V. Dubonos, I. V. Grigorieva, A. A. Firsov, *Science* **2004**, *306*, 666.
[4] K. S. Novoselov, A. K. Geim, S. V. Morozov, D. Jiang, M. I. Katsnelson, I. V. Grigorieva, S. V. Dubonos, A. A. Firsov, *Nature* **2005**, *438*, 197.
[5] K. I. Bolotin, K. J. Sikes, Z. Jiang, M. Klima, G. Fudenberg, J. Hone, P. Kim, H. L. Stormer, *Solid State Commun.* **2008**, *146*, 351.
[6] A. A. Balandin, S. Ghosh, W. Bao, I. Calizo, D. Teweldebrhan, F. Miao, C. N. Lau, *NanoLett.* **2008**, *8*, 902.
[7] M. Chhowalla, H. S. Shin, G. Eda, L. J. Li, K. P. Loh, H. Zhang, *Nat. Chem.* **2013**, *5*, 263.
[8] M. Osada, T. Sasaki, *J. Mater. Chem.* **2009**, *19*, 2503.
[9] Q. H. Wang, K. Kalantar-Zadeh, A. Kis, J. N. Coleman, M. S. Strano, *Nat. Nanotechnol.* **2012**, *7*, 699.
[10] A. Castellanos-Gomez, L. Vicarelli, E. Prada, J. O. Island, K. L. Narasimha-Acharya, S. I. Blanter, D. J. Groenendijk, M. Buscema, G. A. Steele, J. V. Alvarez, H. W. Zandbergen, J. J. Palacios, H. S. J. van der Zant, *2D Mater.* **2014**, *1*, 025–001.
[11] A. C. Ferrari, J. C. Meyer, V. Scardaci, C. Casiraghi, M. Lazzeri, F. Mauri, S. Piscanec, D. Jiang, K. S. Novoselov, S. Roth, A. K. Geim, *Phys. Rev. Lett.* **2006**, *97*, 187–401.
[12] Y. N. Xu, D. Zhan, L. Liu, H. Suo, Z. H. Ni, T. T. Nguyen, C. Zhao, Z. X. Shen, *ACS Nano* **2011**, *5*, 147.

© 2015 WILEY-VCH Verlag GmbH & Co. KGaA, Weinheim

[13] Z. H. Ni, T. Yu, Y. H. Lu, Y. Y. Wang, Y. P. Feng, Z. X. Shen, *ACS Nano* **2008**, *2*, 2301.
[14] C. Rice, R. J. Young, R. Zan, U. Bangert, D. Wolverson, T. Georgiou, R. Jalil, K. S. Novoselov, *Phys. Rev. B* **2013**, *87*, 081-307.
[15] L. Li, Y. Yu, G. J. Ye, Q. Ge, X. Qu, H. Wu, D. Feng, X. H. Chen, Y. Zhang, *Nat. Nanotechnol.* **2014**, *9*, 372.
[16] F. Xia, H. Wang, Y. Jia, *Nat. Commun.* **2014**, *5*, 4458.
[17] H. Liu, A. Neal, Z. Zhu, L. Luo, X. Xu, D. Tomanek, P. Ye, *ACS Nano* **2014**, *8*, 4033.
[18] H. Churchill, P. Jarillo-Herrero, *Nat. Nanotechol.* **2014**, *9*, 330.
[19] S. Koenig, R. Doganov, H. Schmidt, A. H. Castro Neto, B. Ozyilmaz, *Appl. Phys. Lett.* **2014**, *104*, 103–106.
[20] A. S. Rodin, A. Carvalho, A. H. Castro Neto, *Phys. Rev. Lett.* **2014**, *112*, 176–801.
[21] M. Buscema, D. J. Groenendijk, S. I. Blanter, G. A. Steele, H. S. J. van der Zant, A. Castellanos-Gomez, *Nano Lett.* **2014**, *14*, 3347.
[22] V. Tran, R. Soklaski, Y. Liang, L. Yang, *Phys. Rev. B* **2014**, *89*, 235–319.
[23] J. Qiao, X. Kong, Z. Hu. F. Yang, W. Ji, *Nat. Commun.* **2014**, *5*, 4475.
[24] H. Liu, Y. Du, Y. Deng, P. D. Ye, *Chem. Soc. Rev.* **2015**, *44*, 2732.
[25] J. Wu, N. Mao, L. Xie, H. Xu, J. Zhang, *Angew. Chem. Int. Ed.* **2015**, *54*, 2366.
[26] R. Fei, L. Yang, *Appl. Phys. Lett.* **2014**, *105*, 083–120.
[27] A. Favron, E. Gaufres, F. Fossard, A. Phaneuf-L'Heureux, N. Y. Tang, P. L. Levesque, A. Loiseau, R. Leonelli, S. Francoeur, R. Martel, *Nat. Mater.* **2015**, *14*, 826.
[28] S. Zhang, J. Yang, R. Xu, F. Wang, W. Li, M. Ghufran, Y. Zhang, Z. Yu, G. Zhang, Q. Qin, Y. Lu, *ACS Nano* **2014**, *8*, 9590.
[29] H. B. Ribeiro, M. A. Pimenta, C. J. S. de Matos, R. L. Moreira, A. S. Rodin, J. D. Zapata, E. A. T. de Souza, A. H. Castro Neto, *ACS Nano* **2015**, *9*, 4270.
[30] J. R. Brent, N. Savjani, E. A. Lewis, S. J. Haigh, D. J. Lewis, P. O'Brien, *Chem. Commun.* **2014**, *50*, 13338.
[31] J. N. Coleman, M. Lotya, A. O'Neill, S. D. Bergin, P. J. King, U. Khan, K. Young, A. Gaucher, S. De, R. J. Smith, I. V. Shvets, S. K. Arora, G. Stanton, H. Kim, K. Lee, G. T. Kim, G. S. Duesberg, T. Hallam, J. J. Boland, J. J. Wang, J. F. Donegan, J. C. Grunlan, G. Moriarty, A. Shmeliov, R. J. Nicholls, J. M. Perkins, E. M. Grieveson, K. Theuwissen, D. W. McComb, P. D. Nellist, V. Nicolosi, *Science* **2011**, *331*, 568.
[32] R. Hultgren, N. S. Gingrich, B. E. Warren, *J. Chem. Phys.* **1935**, *3*, 351.
[33] Y. Feng, J. Zhou, Y. Du, F. Miao, C. Duan, B. Wang, X. Wan, *J. Phys.: Condens. Matter* **2015**, *27*, 185–302.
[34] X. Zhang, H. Xie, Z. Liu, C. Tan, Z. Luo, H. Li, J. Lin, L. Sun, W. Chen, Z. Xu, L. Xie, W. Huang, H. Zhang, *Angew. Chem. Int. Ed.* **2015**, *54*, 3633.
[35] M. S. Bahae, A. A. Said, T. H. Wei, D. J. Hagan, E. W. V. Stryland, *IEEE J. Quantum Electron.* **1990**, *26*, 760.
[36] H. Zhang, S. B. Lu, J. Zheng, J. Du, S. C. Wen, D. Y. Tang, K. P. Loh, *Opt. Express* **2014**, *22*, 7249.
[37] E. Garmire, *IEEE J. Sel. Top. Quantum Electron.* **2000**, *6*, 1094.
[38] Q. Bao, H. Zhang,Y. Wang, Z. Ni, Y. Yan, Z. X. Shen, K. P. Loh, D. Y. Tang, *Adv. Funct. Mater.* **2010**, *19*, 3077.

© 2015 WILEY-VCH Verlag GmbH & Co. KGaA, Weinheim